Toward Active Cannulas: Miniature Snake-Like Surgical Robots

Robert J. Webster III,* Allison M. Okamura, and Noah J. Cowan
Department of Mechanical Engineering
The Johns Hopkins University
Baltimore, Maryland 21218-2681
*Corresponding Author: robert.webster@jhu.edu

***Abstract*— We have developed a new class of continuously flexible snake-like robots, called active cannulas, that consist of several telescoping pre-curved superelastic tubes. The devices derive bending actuation not from tendon wires or other external mechanisms, but from elastic energy stored in the backbone itself. This allows active cannulas to have a small diameter and a high degree of dexterity, which should enable them to navigate through complex anatomy to sites inaccessible by current surgical robotic devices. Active cannulas may also enhance patient safety because their inherent compliance mitigates potential trauma from inadvertent tool-tissue collision. A consequence of our design is that dexterity *improves* with miniaturization. A kinematic description of active cannula shape requires a model of the elastic interaction of telescoping pre-curved flexible tubes, and we derive a two-"link" beam mechanics-based model. Experiments using curved nitinol tubes and wires validate the model.**

I. Introduction

While the minimally invasive surgery (MIS) revolution has profoundly improved a variety of surgical interventions, many diseases lack viable MIS alternatives because instruments cannot reach them. This is often due to entry pathways being very small or requiring navigation of challenging 3D geometry. Dexterity must also be maintained after reaching the surgical site to allow surgery to proceed. These constraints render such confined surgical sites off-limits to current commercial surgical robots, as well as manual MIS instruments. New MIS tools are needed that are both smaller and more dexterous than existing devices.

We propose a new type of "snake-like" miniature flexible active cannula that derives bending actuation not from tendon wires or other external mechanisms, but from elastic energy stored in the backbone itself. Differing from traditional MIS tools, which are essentially rigid cylindrical rods (possibly with wrists at the end), active cannulas are sufficiently flexible and shapable to navigate through bends such as those found when traversing the natural orifices, lumens, and other anatomical spaces of the human body. The active cannula design is particularly advantageous because dexterity *improves* with miniaturization. Moreover, inherent (and also somewhat tunable) compliance makes active cannulas safer than existing MIS tools. If inadvertent tissue contact along the shaft occurs, the device will bend rather than damage the tissue. We envision our active cannulas as a family of both hand-held and robotic devices tailored to meet various clinical needs. A fully robotic version could be used as a new kind of slave robot in a telesurgical system like those commercially available today.

Active cannulas are relevant for a wide range of challenging surgical applications. For example, the least invasive treatments for tumors or other disease at the base of the skull are performed endoscopically through the nose, and are very difficult because of the winding passages and small openings involved. Two specific surgical sites that cannot be reached using straight tools are the areas behind the carotid arteries (near the base of the eye), and the frontal sinus cavities (one must reach around the bone behind the bridge of the nose) [3]. Other potential active cannula applications include throat surgery [18], transgastric surgery, and fetal surgery, all of which require require dexterity after tool shafts travel long distances and/or are constrained by tissue.

II. Related Work

Hand-held laparoscopic MIS tools generally consist of long, stiff, cylindrical shafts with small tools (grippers, scissors, etc.) on the distal end. Two important advances in MIS tool design have been the addition of a wrist at the end of the tool (enhancing dexterity), and the use of robots to register the tool to the endoscope image (making a teleoperated system easier to use), e.g. [11]. Commercial teleoperated surgical robotics typically use 5-10 mm straight, rigid tools equipped with small wire or push-rod actuated wrists. While no universally agreed upon analytical wrist optimization framework for surgical robots currently exists, preliminary analytical methods indicate that snake-like wrists have advantages over traditional jointed wrist designs [9], [15].

Regardless of wrist design, a major limitation of existing MIS tools is that they are constrained to pivot at the body entry point. While optimal port placement seeks to allow reasonable workspace volume under this constraint [1], [4], there is little flexibility in port placement in applications such as throat or sinus surgery. This motivates our desire to move away from straight rigid tools toward actively shapable flexible instruments.

A. Steering Via Pre-Curvature

The idea of steering the surgical tool via pushing and rotating a pre-curved tip is a powerful one, as evidenced by the ubiquitous adoption of catheters in circulatory procedures.

In catheterization, the guide wire (equipped with a small superelastic curved tip) is navigated through the circulatory system by externally translating and rotating the back end. It steers by using blood vessel reaction forces to bend the flexible catheter around corners. Recently several groups have successfully adapted this "catheter-like" steering strategy in a variety of ways to an entirely different kind of surgery. These groups have developed needles capable of steering through soft tissue using reaction forces from the tissue to bend the needle. The design most like the traditional catheter incorporates a pre-curved stylus that can extend from the tip of a stiffer straight outer cannula [17]. Other examples add pre-curvature also to their outer cannulas [7], [10], [14]. Incorporating optional pre-curvature, our previous work on steerable needles uses the same catheter-like input degrees of freedom (externally controlling push and axial rotation of the back end of the tool), but derives bending actuation primarily from the asymmetry of the standard bevel tip [20], [21].

Inspired by our experience with these steerable needle systems, our Active Cannula system seeks to generalize the catheter-like steering technique to work in free space, without requiring tissue reaction forces to bend the device. We also build on existing needle design ideas by adding more cannulas that can each be individually pushed and rotated with respect to one another.

B. Snake-Like Robots for Surgery

The study of snake-like robots has a long history, and many different designs have been developed. A great deal of pioneering design work was done by Hirose [12], and other designs using binary actuation [5] and tendon driven strategies (e.g. [19]) have been developed more recently. While many of these robots are large and not targeted at medical applications, there have been noteworthy efforts made to miniaturize snake-like robots to a size suitable for use in surgery. However, the pervasive assumption in these efforts has been that the device must begin fundamentally straight, and a force must be generated to bend it. In keeping with this, researchers have developed heat-activated shape-memory-alloy (SMA) devices (e.g. [2], [16]). While many of the existing SMA designs are very creative, SMA actuation faces inherent difficulties with heat dissipation, which can limit band-width and potentially slow the surgery. Other notable designs have incorporated tendons or backbones that apply force to support disks to achieve changes in curvature [6], [18], [19]. While these external wires and push rods allow direct control of curvature, they also limit miniaturization, prompting our desire to build the bending actuation directly into the backbone itself.

In comparison to previous systems, our active cannulas can be smaller and incorporate more bending sections. The initial prototype (Figure 1) is made of pre-curved nitinol tubes and has three sections (more can be created by adding additional tubes), with a largest section diameter of 2.4 mm, tapering to a smallest section diameter of 0.8 mm. Miniaturization of the initial prototype active cannula is possible and straightforward (smaller diameter tubes), and will enhance dexterity as described in Section III. While our prototype is made of the superelastic metal nitinol, active cannulas may be made of any elastic material, including plastics, and their compliance tuned by adjusting tube materials, diameters, and wall thicknesses. While the prototype active cannula described in this paper makes use of only the superelastic properties of nitinol, it is worth noting that if suitable heat transmission mechanisms are used, the design may be able to simultaneously take advantage of both the superelastic and shape memory effects of nitinol.

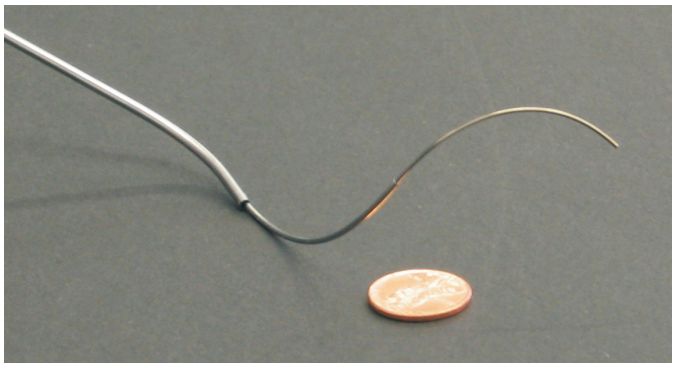

Fig. 1. Prototype active cannula made of superelastic nitinol tubes.

There are two other particularly interesting theoretical features of the active cannula compared to other snake-like robot designs. First, it is often convenient to model a snake-like robot as a mathematical curve (e.g. a series of circular arcs, etc.) [13]. The robot is approximated (more or less accurately depending on the robot and the configuration) as the curve, from a kinematic viewpoint. However, with the active cannula's circular pre-curvatures, no approximation is needed - it will actually be a series of circular arcs. Second, when representing the robot as a mathematical curve, it can be quite challenging to fully describe the effect of physical joint limits, and the robot may inadvertently damage itself [13]. The properly designed active cannula (Section III) is not subject to this danger, since it combines both elastic elements and force transmission elements directly into the extensible backbone. Active cannulas have no joint limits and no danger of self-damage anywhere in their configuration spaces. Any joint limits that are present are an artifact of the specific actuation unit designs, which can in principle be re-designed to allow as much motion as desired.

III. Cannula Design and In-Plane Mechanics

The central idea of the active cannula is the pre-curvature of the component tubes. In this paper we will consider only circular pre-curvature, which simplifies analysis and design. However, other shapes may be suited to specific surgical interventions.

As mentioned above, our prototype active cannula (Figure 1) is composed of concentric superelastic tubes, each with a preset circular shape. The tubes are able to retract and extend relative to one another, as well as rotate axially with respect to one another. In so doing, they change the shape of

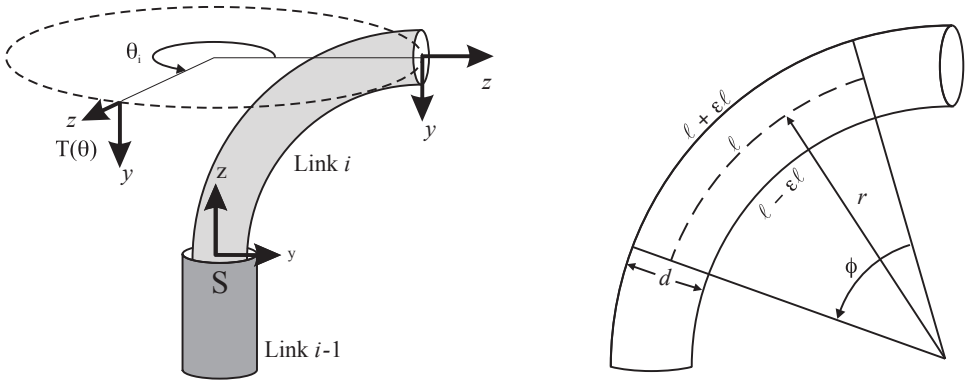

Fig. 2. (Left) Coordinate frames associated with extension and axial rotation of a curved tube. (Right) This diagram demonstrates how tube wall lengths relate to strain.

the cannula. Our prototype device has 6 actuable degrees of freedom (DOF). Each new tube added to the robot increases the number of actuable DOF by two (one DOF extension and one DOF rotation). Before directly addressing models of tube interaction as these DOF are actuated, we examine the design of tube pre-curvature.

A. Maximum Pre-Curvature for a Single Tube

One design decision that must be carefully made is the selection of the initial curvature to be pre-set into each tube. In the absence of specific clinical requirements, smaller radii of pre-curvature are generally desirable, since they enable the cannula to negotiate tighter turns within anatomy. However, if the radii of pre-curvature are chosen too small, the cannula may damage itself (plastically deforming one or more of its component tubes) at certain positions in its configuration space.

While some medical interventions may not require access to the full configuration space (for example, one or more tubes may not be required to perform 360° rotations) and thus permit smaller radii of curvature, it is generally desirable to design tube pre-curvatures to avoid active cannula self-damage. This is accomplished by ensuring that the maximum strain in all component tubes is maintained within the elastic region for all possible robot configurations. Since superelastic materials can sustain high strain without plastic deformation, we selected nitinol (a superelastic alloy of nickel and titanium) as the material for the tubes in our initial prototype. Nitinol has been reported to sustain recoverable strains of as much as $\varepsilon = 11\%$ [8], but most estimates place recoverable strain near 8%.

For small diameter tubes, this corresponds to a large curvature, or equivalently a small radius of curvature. Figure 2 (Right) shows a small section of initially straight tube that is curved into a circular shape by an external force distribution (not pictured). The midline length is ℓ as are the initial lengths of the top and bottom surfaces of the tube. When the initially straight tube is bent into the circular shape shown, the top and bottom surfaces are lengthened and shortened, respectively, by a fraction ε of their initial length. The arc length ℓ of a section of radius r and angle ϕ is given by $\ell = r\phi$. The arc length of the bottom surface of the tube is thus given by

$$\ell - \varepsilon\ell = \left(r - \frac{d}{2}\right)\phi. \tag{1}$$

Substituting $\frac{\ell}{r}$ for ϕ and simplifying, we arrive at an expression for the radius of curvature as a function of strain,

$$r = \frac{d}{2\varepsilon} \quad \text{or} \quad \kappa = \frac{2\varepsilon}{d}. \tag{2}$$

Thus, using 8% strain ($\varepsilon = 0.08$) and a 1 mm tube, the minimum possible circular radius around which it is possible to deflect a straight nitinol tube without plastic deformation is 6.25 mm.

The situation is slightly different when one considers straightening an initially curved tube (rather than curving an initially straight tube). In this case, the bottom surface begins shorter than the top surface, and so reaches its strain limit first. However, accounting for this requires only a minor modification to the above analysis, and one can show that the minimum radius of curvature is now

$$r = \frac{d}{2\varepsilon} + \frac{d}{2} \quad \text{or} \quad \kappa = \frac{2\varepsilon}{d(1+\varepsilon)}. \tag{3}$$

In either case, the curvature of the tube is inversely proportional to tube outer diameter d. Thus, smaller tubes can sustain higher pre-set curvatures. This means that as the design is miniaturized, it will be able to reach around tighter corners, enhancing its dexterity. The tradeoff for enhancing dexterity in this manner is a reduction in stiffness and/or in the size of the central working channel.

Other design considerations may necessitate choosing a curvature somewhat less than this maximum value. For example, finite torsional stiffness means that if a tube is expected to rotate 360° within another smoothly (with acceptable hysteretic motion and elasticity release near the "singularity" at 180°), one may have to choose a curvature less than the theoretical maximum for each tube. We address this torsional issue further in Section IV.

When designing to avoid cannula self-damage, another reason for choosing a curvature slightly less than the theoretical

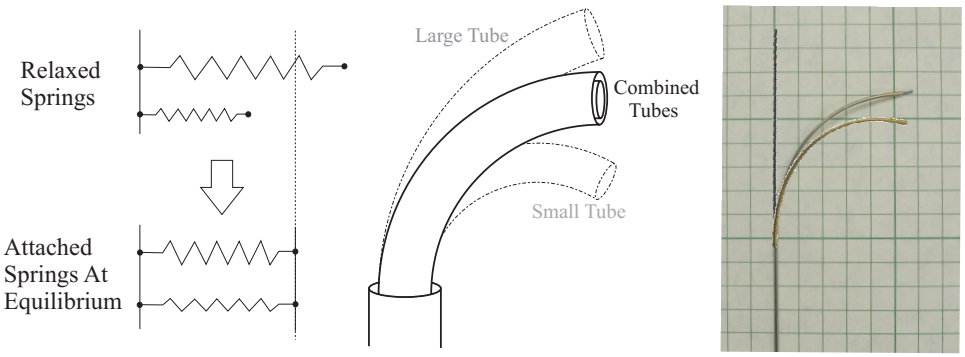

Fig. 3. (Left) Parallel spring position equilibrium. (Middle) Analogous curved tube equilibrium. Dashed lines indicate natural tube curvatures, solid lines show the effect of placing tubes inside one another. (Right) Photograph of experiment. Initially straight wire and initially curved tube shapes are superimposed on a photograph of the combined wire and tube.

maximum is that generally one or more tubes in the active cannula will have to bend back on themselves (i.e. further than straight). To evaluate the design implications of this (Sec. III-C), we must first examine the effect of pre-curved coplanar tubes on one another.

B. In-Plane Beam Mechanics

If several pre-curved tubes are placed concentrically, their curvatures will interfere with one another, making the combined shape different from the natural rest shapes of the individual tubes. It is this interference effect, combined with both rotation and extension and retraction of the tubes, that we use to change the shape of the active cannula. To describe the complete shape of the active cannula, we must first develop a model for the shape of a single unique region of tube overlap. Each region will have an associated curvature and plane in which it bends.

Figure 3 shows the effect concentric tubes of different pre-curvatures have on one another in the planar case. Here, the tubes have not been axially rotated with respect to one another and their natural bending planes line up. The Bernoulli-Euler beam equation describes the instantaneous curvature of a beam with respect to arc length as

$$\kappa = \frac{d\phi}{ds} = \frac{M}{EI}, \tag{4}$$

where ϕ is the angle measured from the tangent vector, s is arc length, M is the moment applied to a differential element, E is the Modulus of Elasticity (Young's Modulus), and I is the cross sectional moment of inertia of the tube.

Using circular pre-set tube curvatures permits an idealization of the beam equation. Because the curvature is constant for each tube, the tube will apply a constant moment on the tubes exterior to or within it, namely:

$$M = EI\Delta\kappa \tag{5}$$

If the tubes are axially aligned so that they naturally curve in the same plane, (5) is analogous to Hooke's law for a linear spring, i.e. "$F = k\Delta x$", as illustrated in Figure 3. In the analogy, the bending stiffness, EI, of a tube corresponds to the spring constant, the moment, M, corresponds to the linear force, and the "position" variable, κ, describes the curvature of a tube. Just as we can describe the equilibrium position of linear springs of different lengths in parallel by a force balance, we can describe the resultant curvature of two overlapping tubes by

$$\kappa_{eq} = \frac{I_1\kappa_1 + I_2\kappa_2}{I_1 + I_2} \quad \text{or} \quad \kappa_{eq} = \frac{\sum_{i=1}^{n} I_i\kappa_i}{\sum_{i=1}^{n} I_i} \tag{6}$$

for n tubes. This model is verified experimentally in Section III-D.

C. Design Implications of Tube Interaction

Rotating one tube 180° with respect to the other is analogous to attaching a linear spring to the other side of the wall, so that its initial position is now $-x$ ($-\kappa$ for the tube). Thus the equilibrium position of the softer of the two springs will, in general, be on the opposite side of zero from where it begins. For the tubes, this corresponds to bending further than straight (further than zero curvature). We can define $\Delta\kappa_{\max}$ for each tube as $\Delta\kappa_{\max} = \kappa_o - \min(\kappa_{eq})$. The minimum κ_{eq} will occur when all other tubes are rotated 180° with respect to the tube in question. The $\Delta\kappa_{\max}$ values for each tube must be kept at or below the bounds in (3), to prevent the possibility of plastic deformation in any tube for all possible active cannula configurations.

D. Experimental Model Validation

We experimentally validated the in-plane beam mechanics model using curved nitinol tubes and straight wires as shown

Tube			Wire		Combined	
ID (mm)	OD (mm)	κ (1/mm)	OD (mm)	κ (1/mm)	r meas (mm)	r pred (mm)
0.622	0.800	0.044	0.43	0.0	26.0	25.5
0.965	1.27	0.020	0.8	0.0	62.5	61.2
1.47	1.78	0.021	1.2954	0.0	75.5	72.8
2.01	2.39	0.028	1.6002	0.0	49.8	50.5

TABLE I

VERIFICATION OF BERNOULLI-EULER BASED BEAM MECHANICS MODEL.

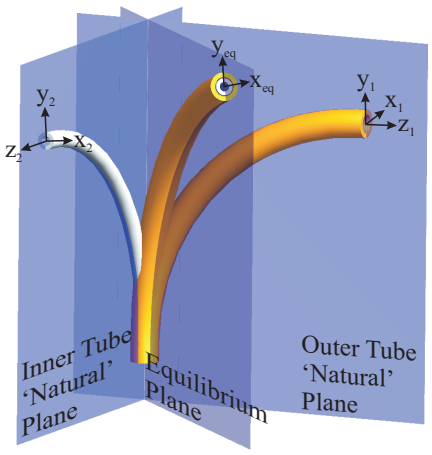

Fig. 4. If two concentric curved tubes are axially rotated with respect to one another, they will reach a minimum energy equilibrium between the planes they would independently bend in (their "natural" planes). They will also cause one another to straighten from their "natural" pre-set curvatures.

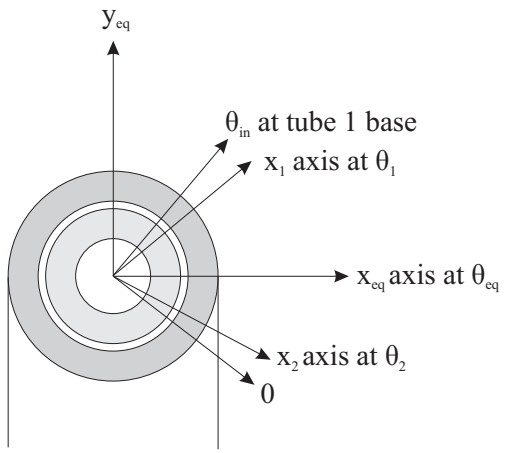

Fig. 5. End-on view of tube tips in at equilibrium, illustrating the rotation of the coordinate frames in Figure 4 as the outer tube rotates with respect to the inner tube. The angle θ_2 and the difference between θ_{in} and θ_1 are a result of torsional deformation in the straight tube sections between the actuators and the curved sections.

in Figure 3. Table I illustrates our results. The nitinol tubes were plastically deformed to an initial curvature κ_t. The wires were initially straight, with $\kappa_w = 0$. The model prediction is given by Equation 6. Data was collected as shown in Figure 3. Photographs of the tubes were taken against the 5 mm grid both before and after the wires were inserted. The best-fit circle was then determined manually by examining the photographs and adjusting the diameter of a fitting circle until it closely matched the curvature in the photograph.

It is challenging to plastically deform a superelastic alloy such as nitinol. Because of this, the arc length on some specimens was rather short (as little as 1.5 cm, in the case of tube 3). The error associated with fitting a circle to so small an arc could potentially be as much as 8-10% of the actual circle radius. It would be preferable to have nitinol pre-shaped by the manufacturer in the desired circular shape, but this would have added tremendous cost at the very small quantities used in this study. It may also be possible to heat set a curvature into straight nitinol tubes after purchase, but our efforts to do so led to destruction of the superelastic properties of the nitinol and very rapid fatigue failure. Nitinol requires a specific heat-time profile to set a shape while retaining superelasticity, and our heat treatment attempts, while successful in setting desired shape, did not yield superelastic specimens.

IV. Axial Tube Rotation

When curved tubes are rotated axially, their natural planes of curvature are no longer aligned and the direction of the bending moments they apply changes. In addition to bending moments, a torsional force is also generated by such motion. We will begin in this section by considering bending only, and proceed to incorporate torsion to the model in Section IV-B.

A. Bending Model

Intuitively, if two pre-curved tubes with same stiffness (EI) and initial curvature κ are placed within one another and rotated $90°$ with respect to one another, we expect the combined tubes to exhibit a bending plane directly between them, at $45°$, and to straighten out somewhat (at $180°$ they would be completely straight). This is illustrated in Figure 4. If the tubes do not have the same stiffness, then the combined bending plane will shift toward the stiffer tube.

This intuition can be formalized in terms of the Bernoulli-Euler beam mechanics described earlier. Tubes whose natural bending planes are rotated with respect to one another exert a moment on one another around their respective x axes, caused by their initial pre-curvature about this direction. Figure 5 shows an end-on view of the tubes inside one another at equilibrium in their combined bending plane. The exterior tube (tube 1) has been rotated about its base through an angle θ_{in} with respect to the inner tube (tube 2). The coordinate frames attached to the tubes are as in Figure 4.

As mentioned before, $M = EI(\Delta\kappa)$, but now this moment has two component projections on the equilibrium x and y axes. Summing the moments about the equilibrium x axis yields

$$\kappa_x = \frac{EI_1 \cos(\theta_1 - \theta_{\text{eq}})\kappa_1 + EI_2 \cos(\theta_{\text{eq}} - \theta_2)\kappa_2}{EI_1 + EI_2}, \qquad (7)$$

the equilibrium curvature of the tubes in the combined bending plane. Similarly,

$$\kappa_y = \frac{EI_1 \sin(\theta_1 - \theta_{\text{eq}})\kappa_1 + EI_2 \sin(\theta_{\text{eq}} - \theta_2)\kappa_2}{EI_1 + EI_2}. \qquad (8)$$

These curvatures can be generalized for more than one tube as was done in (6).

We conjecture, and have experimentally observed, that the tubes reach an equilibrium where $\kappa_y = 0$ (though we do

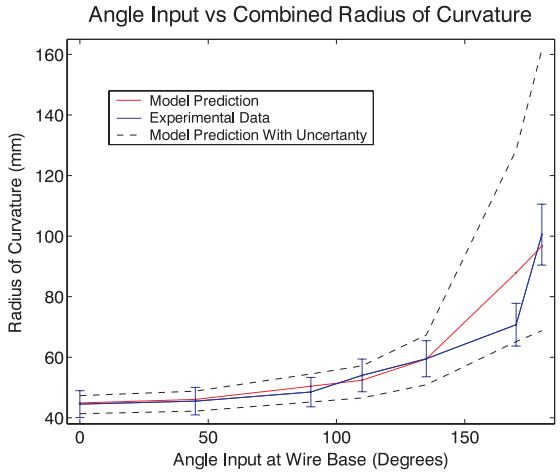

Fig. 6. Model prediction and experimental combined radius of curvature are are similar over a wide range of input angles. The inclusion of manufacturing tolerances and estimated measurement error in natural tube and wire curvatures yield the dashed curves. Error bars on experimental data show estimated error in combined radius of curvature measurements.

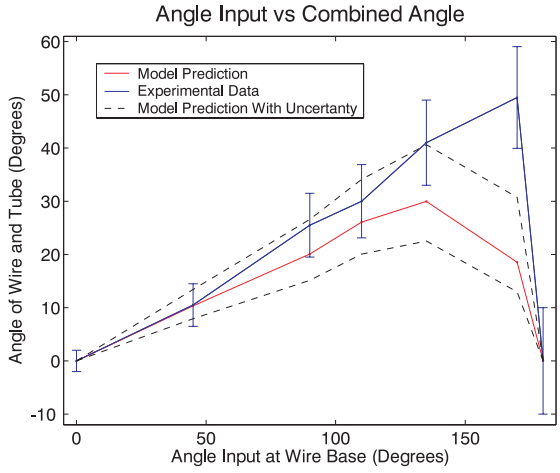

Fig. 7. Model prediction and experimental equilibrium angle are similar over a wide range of input angles. The inclusion of manufacturing tolerances and estimated measurement error in natural tube and wire curvatures yield the dashed curves. Error bars on experimental data show estimated error in equilibrium plane measurements.

not formally show this here). Under this assumption, it is possible to solve for the θ_{eq} in (8) to determine the angle of the combined bending plane. In the absence of torsion, this would be sufficient to describe the shape of combined tubes. However, torsional deformation will also occur, particularly in the straight regions of the tubes leading up to the curved sections as shown in Figure 1. Thus, we will solve for equilibrium curvature and combined bending plane not through numerical evaluation of Equation 8, but rather by determining the minimum energy configuration for the tubes in the presence of both transmissional torsion and bending of the curved sections.

B. Torsion in Transmission

In contrast to bending moments, axial torsional moments generated by tube interaction will not be constant along the curved sections of the tubes. The torsional moment will be zero at the tip, and build to a maximum value at the base of the curved section. Since torsional deformation is directly proportional to length and the straight portions of the tubes between the actuators and the curved sections are much longer than the curved sections themselves, much of the torsional deformation will occur along the straight part of the shaft. Assuming that the straight segment deformation dominates the torsional effects, it is possible to express the total energy in the system in terms of the torsional energy stored in linear region of the tubes and the bending energy stored in the curved sections:

$$
\begin{aligned}
E(q) = \frac{GJ_2}{2L_2}\theta_2^2 + \frac{GJ_1}{2L_1}(\theta_{\text{in}} - \theta_1)^2 \\
+ \frac{EI_2\ell_2}{2}(\kappa_x - \kappa_2\cos(\theta_{\text{eq}} - \theta_2))^2 \\
+ \frac{EI_1\ell_1}{2}(\kappa_x - \kappa_1\cos(\theta_1 - \theta_{\text{eq}}))^2 \\
+ \frac{EI_2\ell_2}{2}(\kappa_2\sin(\theta_{\text{eq}} - \theta_2))^2 \\
+ \frac{EI_1\ell_1}{2}(\kappa_1\sin(\theta_1 - \theta_{\text{eq}}))^2,
\end{aligned}
$$

where G is the shear modulus, J is the polar moment of inertia, ℓ is the length of the curved section of each tube and L is the length of the straight section between the actuator and the curved part of the tube. For a given input angle, the total energy $E(q)$ is a function of three variables $q = (\theta_1, \theta_2, \theta_{\text{eq}})$. Using gradient decent, it is possible to find the minimum energy shape of the active cannula with respect to q. The shape of the cannula is then given by θ_{eq} and $\kappa_x(q)$ given in (7).

C. Rotational Experimental Validation

To experimentally validate the rotational model, an initially straight tube (ID = 2.01 mm, OD = 2.39 mm) was plastically deformed to a curvature of 0.0263/mm. An initially slightly curved wire (OD = 1.778 mm, $\kappa_o = 0.00669/\text{mm}$) was plastically deformed to a curvature of 0.0157/mm. The arc length where the curved portions of the tube and wire interacted was $\ell_c = 27.5\text{mm}$.

For experimental input angles $0-90°$, the tube was attached using Loctite 408 instant adhesive to an acrylic fixture with L = 16 mm. At this point the adhesive bond broke due to fatigue, and the tube was re-glued with L = 28 mm for the remaining input angles. The wire was inserted into the tube and the L from the grip point to the curved region was measured at $L_0 =$

49, $L_{45} = 49$, $L_{90} = 49, L_{110} = 58$, $L_{135} = 56$, $L_{170} = 53$, and $L_{180} = 58$, where the subscripts denote the input angle.

The experiment proceeded as follows. The wire was rotated through a distance θ_{in}, as measured by a protractor, and held constant. A flat planar grid was placed behind the tube and wire, and a photograph was taken. This equilibrium plane was also measured with respect to the $\theta_{\text{in}} = 0$ plane using a protractor. We estimate the error in this angular measurement to vary approximately linearly, from approximately 2° to 10° with input angle. When curvature was largest, measurements were more accurate, because the equilibrium bending plane was easier to observe. As the cannula straightened as θ_{in} approached 180°, the combined bending plane was more difficult to measure. Curvatures for each input angle were obtained from the photographs using the procedure described in Section III-D.

The results are as shown on Figures 6 and 7. The prediction with uncertainty plots were generated by including manufacturing tolerances of 0.0254 mm for the tube and wire diameters as well as measurement errors of 10% for the initial radii of curvature of the tube and wire. The error bars on the experimental data show the effect of 10% error in radius of curvature measurements at each experimental data point.

V. Conclusions and Future Work

Miniature flexible robots like our active cannulas are a means to bring the benefits of MIS to difficult-to-reach locations in the human body as well as to enhance patient safety. By building pre-curvature into the tubes that form the backbone, active cannulas can (1) be very small in diameter, (2) have many snake-like bending sections with little mechanical complexity, (3) use high band-width actuators (DC motors), and (4) have improved dexterity with miniaturization.

This paper takes initial steps toward realizing the potential of active cannulas. Our analysis of elastic deformation limits provides design guidelines for active cannula pre-curvatures, and our beam mechanics-based model of tube interaction can be used to generate a kinematic model. Experiments show that considering curved tube bending along with torsional deformation in straight transmission regions is sufficient to describe tube behavior well through large angles of rotation. At very large angles near the "singularity" at 180°, unmodeled factors such as torsion in curved sections and frictional effects become stronger. Of these, our experience suggests that torsion may be more significant, since our experiments were easily carried out without lubrication.

We expect that active cannulas will eventually become a diverse family of surgical devices, both manual and robotic, with the potential to extend the reach of MIS to confined areas of the body. A fully robotic teleoperated active cannula might also incorporate algorithms (currently under development at JHU and elsewhere) on cooperative assistance algorithms embedded in the controller, motion scaling, and tremor cancelation. Eventually a complete system may also assist in path planning, and incorporate information from preoperative medical images into the surgery. In short, we believe that active cannulas have the potential to bring all the advantages of computer assisted surgery to bear on many surgical sites that are inaccessible today.

Acknowledgment

This work was supported in part by an National Defense Science and Engineering Graduate Fellowship and The Johns Hopkins University. The authors thank Dr. Nabil Simaan for discussions on snake robot design.

References

[1] L. Adhami and E. Coste-Maniere. Optimal planning for minimally invasive surgical robots. *IEEE Trans. Rob. Autom.*, 19(5):854–863, 2003.

[2] S. Aramaki, S. Kaneko, K. Arai, Y. Takahashi, H. Adachi, and K. Yanagisawa. Tube type micro manipulator using shape memory alloy (sma). *Int. Symp. Micro Machine and Human Science*, pages 115–120, 1995.

[3] M. C. Snyderman. Co-director, Center for Minimally Invasive and Cranial Base Neurosurgery, University of Pittsburgh Medical Center. Personal Communication, 2004.

[4] J. W. Cannon, J. A. Stoll, S. D. Sehla, P. E. Dupont, R. D. Howe, and D. F. Torchina. Port placement planning in robot-assisted coronary artery bypass. *IEEE Trans. Rob. Autom.*, 19(5):912–917, 2003.

[5] G. Chirikjian. A binary paradigm for robotic manipulators. *IEEE Int. Conf. Rob. and Autom.*, pages 3063–3069, 1994.

[6] P. Dario, C. Paggetti, N. Troisfontaine, E. Papa, T. Ciucci, M. C. Carrozza, and M. Marcacci. A miniature steerable end-effector for application in an integrated system for computer-assisted arthroscopy. *IEEE Int. Conf. Rob. Autom.*, pages 1573–1579, 1997.

[7] W. Daum. A deflectable needle assembly, 2003. Patent 5,572,593.

[8] T. W. Duerig, A. R. Pelton, and D. Stockel. Superelastic nitinol for medical devices. *Medical Plastics and Biomaterials Magazine*, pages 30–43, March 1997.

[9] A. Faraz and S. Payandeh. Synthesis and workspace study of endoscopic extenders with flexible stem, research report, experimental robotics laboratory. Simon Fraser University, Canada, http://www.ensc.sfu.ca/research/erl/med/. Last accessed 10/4/2005.

[10] J. Furusho, R. Murai, T. Fujimoto, T. Ono, Y. Chiba, and H. Horio. A new medical mechatronics system for percutaneous umbilical blood sampling using curved multi-tube. *CME*, pages 88–92, 2005.

[11] G. S. Guthart and J. K. Salisbury. The Intuitive^{TM} telesurgery system: Overview and application. *IEEE Int. Conf. Rob. Autom.*, pages 618–621, 2000.

[12] S. Hirose. *Biologically Inspired Robots, Snake-Like Locomotors and Manipulators*. Oxford University Press, 1993. pp. 147-154.

[13] B. A. Jones, W. McMahan, and I. D. Walker. Practical kinematics for real-time implimentation of continuum robots. *IEEE Int. Conf. Rob. Autom.*, pages 1840–1847, 2006.

[14] M. Loser. A new robotic system for visually controlled percutaneous interventions under X-ray or CT-fluoroscopy. Master's thesis, Albert Ludwigs University, Freiburg, Germany, September 2002.

[15] F. T. M. Cavusoglu, I. Villanueva. Workspace analysis of robotics manipulators for a teleoperated suturing task. *IEEE/RSJ Int. Conf. Intel. Rob. Sys.*, 4:2234–2239, 2001.

[16] Y. Nakamura, A. Matsui, T. Saito, and K. Yoshimoto. Shape-memory-alloy active forceps for laparoscopic surgery. *IEEE Int. Conf. Rob. Autom.*, pages 2320–2327, 1995.

[17] S. Okazawa, R. Ebrahimi, J. Chuang, S. E. Salcudean, and R. Rohling. Needle insertion modeling and simulation. *IEEE/ASME Trans. Mechatronics*, 10(3):285 – 296, 2005.

[18] N. Simaan, R. Taylor, and P. Flint. A dexterous system for laryngeal surgery. *IEEE Int. Conf. Rob. Autom.*, pages 351–357, 2004.

[19] I. D. Walker. Some issues in creating 'invertebrate' robots. *Int. Symp. Adaptive Motion of Animals and Machines*, 2000.

[20] R. J. Webster III, N. J. Cowan, G. S. Chirikjian, and A. M. Okamura. Nonholonomic modeling of needle steering. *International Journal of Robotics Research*, 25(5/6):509–526, May/June 2006.

[21] R. J. Webster III, J. Memisevic, and A. M. Okamura. Design considerations for robotic needle steering. *IEEE International Conference on Robotics and Automation*, pages 3599–3605, 2005.